Journal of Solid State Chemistry 184 (2011) 786–789

Contents lists available at ScienceDirect

Journal of Solid State Chemistry

journal homepage: www.elsevier.com/locate/jssc

Effect of high hydrostatic pressure on structural stability of Ti_3GeC_2: A first-principles investigation

Shouxin Cui [a,*], Wenxia Feng [a], Haiquan Hu [a], Guiqing Zhang [a], Zengtao Lv [a], Zizheng Gong [b]

[a] School of Physics Science and Information Technology, Liaocheng University, Liaocheng 252059, PR China
[b] Beijing Institute of Spacecraft Environment Engineering, Beijing 100094, PR China

ARTICLE INFO

Article history:
Received 2 November 2010
Received in revised form
28 December 2010
Accepted 7 February 2011
Available online 12 February 2011

Keywords:
Ti_3GeC_2
First principles
Structural stability
Elastic constants
Electronic structure

ABSTRACT

An investigation into the structural stability, electronic and elastic properties of Ti_3GeC_2 under high hydrostatic pressure was conducted using first-principles calculations based on density functional theory (DFT). From the energy and enthalpy calculations, and the variations of elastic constants with pressure, we conclude that α-Ti_3GeC_2 is most stable upon compression to 100 GPa, which is not consistent with the nonhydrostatic *in situ* synchrotron X-ray diffraction studies. The higher structural stability was analyzed in terms of electronic level. The absence of band gap at the Fermi level and the finite value of the density of states at the Fermi energy reveal the metallic behavior of all polymorphs of Ti_3GeC_2.

1. Introduction

The $M_{n+1}AX_n$ (MAX) compounds, where $n=1$, 2, or 3, M is an early transition metal, A is an A-group (mostly IIIA and IVA) element, and X is either C or N, have been studied extensively due to the unusual set of properties. Like metals, they are good thermal and electrical conductors, relative soft (Vickers hardness $\approx 2-5$ GPa) and most readily machinable. Like ceramics, they are also exceedingly damage and thermal shock resistant. According to the value of n, this class of materials form three groups, viz. M_2AX, M_3AX_2, and M_4AX_3. All MAX compounds have highly stable lattices under high pressure [1–4]. As a member of M_3AX_2 compounds, the structural stability of Ti_3SiC_2 has extensively been investigated both experimentally and theoretically. Two structure polymorphs (α- and β-Ti_3 SiC_2) were identified by both X-ray diffraction and high resolution transmission electron microscopy studies [5,6]. Both of them possessed the same space group symmetry, D^4_{6h}-$P6_3/mmc$, but different from each other in Si atoms occupying different positions in the (001) atomic plane. The Si atom in α-Ti_3 SiC_2 occupied a 2*b* Wyckoff position with fractional coordinates (0, 0, 1/4), and in β-Ti_3 SiC_2, it occupied a 2*d* Wyckoff position with fractional coordinates (2/3,1/3,1/4). However, synchrotron X-ray diffraction measurements showed that α-Ti_3 SiC_2 was structurally stable, and no further structural phase transition was observed under pressure up to 61 GPa at room temperature [7]. First principles calculation predicted that the phase transformation (α-to-β) for Ti_3SiC_2 resulted from the large shear strains [8]. With a reference of Ti_3SiC_2,Ti_3GeC_2 is thus expected to have the similar phase transformation under large shear strains, because Ge is larger in ionic radii than Si, and replacement of Ge to Si in the same structure may result in the structural instability of Ti_3GeC_2. The *in situ* synchrotron X-ray diffraction studies revealed that there existed α-to-β-Ti_3GeC_2 phase transition under nonhydrostatic pressure [9]. To our knowledge, there are no experimental and theoretical reports of the phase transition of Ti_3GeC_2 under hydrostatic pressure. Moreover, the elastic properties are very important to understand the phase stability, and there are no reports between them. This provide us with the motivation to undertake a detailed study of the structural stability of Ti_3GeC_2 under hydrostatic pressure by employing the plane-wave pseudopotential method based on DFT.

2. Computational details

The calculations were performed using the plane-wave pseudopotential method as implemented in the CASTEP code [10]. The electronic exchange-correlation interactions were treated by the generalized gradient approximation (GGA) within the scheme due to Perdew–Burke–Ernzerhof (PBE) [11]. The Vanderbilt-type ultrasoft pseudopotentials were employed to model the ion–electron interactions [12]. The states of Ti $3s^23p^63d^24s^2$,

* Corresponding author. Fax: +86 635 8238055.
E-mail address: shouxincui@yahoo.com (S. Cui).

0022-4596/$ - see front matter Crown Copyright © 2011 Published by Elsevier Inc. All rights reserved.
doi:10.1016/j.jssc.2011.02.007

Ge $4s^2 4p^2$ and C $2s^2 2p^2$ were treated as valence states. The integrations over the Brillouin zone (BZ) were replaced by discrete summation over a special set of k points using the Monkhorst–Pack scheme [13]. The energy cutoff of the plane-wave basis was chosen as 550 eV. Large sets of Monkhorst–Pack meshes of $11 \times 11 \times 4$ and $14 \times 14 \times 7$ for α- and β-Ti_3GeC_2, respectively, were used to sample the BZ. The chosen plane-wave cutoff energy and the numbers of k points were carefully checked to ensure good convergence of the computed energies. The convergence tolerance in the self-consistent field calculation is less than 10^{-8} eV Å^{-1}. For a given external hydrostatic pressure, the parameters of both the lattice constants and the internal coordinates of the atoms were fully relaxed until the atomic forces had converged to less than 0.01 eV Å^{-1}. The elastic constants were calculated by the finite-strain technique [14].

3. Results and discussion

3.1. Structural parameter and phase stability

Ti_3GeC_2 possesses the same structure with Ti_3SiC_2, and the detailed description on the geometrical characters of the polymorphs for Ti_3SiC_2 can be found in Refs. [5,6]. The optimized crystal structures of polymorphs for Ti_3GeC_2 at zero pressure are illustrated in Fig. 1. The Ti atoms are labeled Ti1 and Ti2 owning to the structural nonequivalency. The calculated lattice parameters for Ti_3GeC_2 as determined from geometry at zero pressure are given in Table 1, together with the available experimental data. It should be noted that our calculated lattice constants of a and c are in good agreement with experimental values [9], differing only by 0.098% and 0.41%, respectively. The calculated unit-cell volumes at fixed values of applied hydrostatic pressure in the range from 0 to 100 GPa with the step of 10 GPa were used to construct the equation of state (EOS), which was fitted to a third-order Birch–Murnaghan EOS [15], and yielded the bulk modulus (B) and its pressure derivative B'. The calculated B and B' of Ti_3GeC_2 are also listed in Table 1. It can be seen that our calculated B and B' are consistent well with the experimental data [9]. These ensure the reliability of the present first-principles computations.

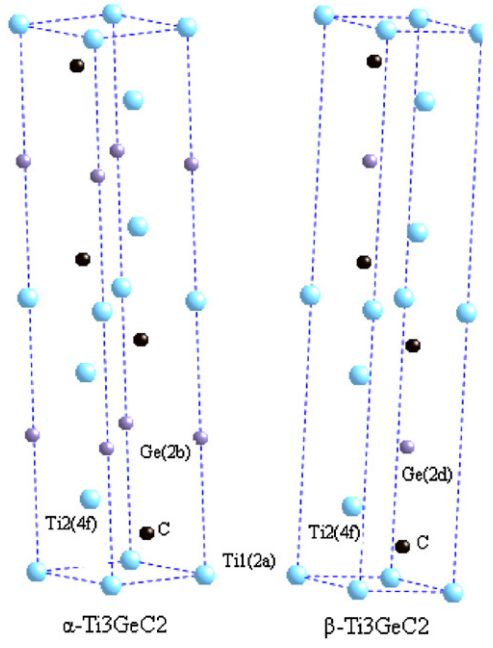

Fig. 1. Crystal structures of the α- and β-Ti_3GeC_2 polymorphs. Species of atoms and corresponding Wyckoff positions are illustrated.

To investigate the possibility of the pressure-induced α-to-β-Ti_3GeC_2 phase transformations, we applied hydrostatic pressure to these two phases of Ti_3GeC_2 compound, and fully optimized both the lattice parameters and the atomic positions, the computed relative energy and enthalpy versus pressure curves for these two phases are shown in Fig. 2. As shown in Fig. 2, there is no point of intersection for these two phases, and the relative energy and enthalpy of β-Ti_3GeC_2 are larger than those of α-Ti_3GeC_2 in the pressure range from 0 to 100 GPa, which indicates that no structural transformations occurred for Ti_3GeC_2, and α-Ti_3GeC_2 is the most stable phase upon compression to 100 GPa, which is not consistent with the nonhydrostatic experimental reports [9]. Thus, the discrepancy between this study and experimental investigation is understandable, our present investigations are conducted under hydrostatic pressure, while the formation of β-Ti_3GeC_2 results from the large shear strain. This is consistent with observation in β-Ti_3 SiC_2 [5,6,8]. In order to meet such a nonhydrostatic condition, experimental measurements were performed without any pressure transmission medium and produce the large pressure gradient.

3.2. Elastic properties

The elastic constants are important parameters that describe the response to an applied macroscopic stress, especially the elastic constants have a close relation with the elastic stability of system being studied. The variations of elastic constants with the pressure for α-Ti_3GeC_2 is indicated in Table 2. For a hexagonal crystal, the mechanical stability under isotropic pressure is

Table 1
Calculated equilibrium lattice constants (Å), bulk modulus B (GPa) and its pressure derivative B' for Ti_3GeC_2 compared with the available experimental values.

	a	c	B	B'
α-Ti_3GeC_2				
Present	3.074	17.686	185.2	4.08
Exp.[a]	3.071	17.759	179 ± 10	4.0
β-Ti_3GeC_2				
Present	3.047	18.089	177.04	4.12

[a] Ref. [9].

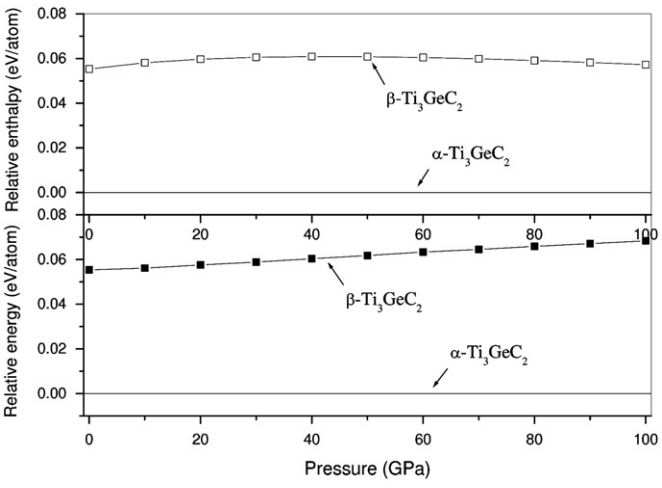

Fig. 2. Calculated enthalpy and energy differences of α- and β-Ti_3GeC_2 as a function of pressure. The α phase has been taken as a reference.

Table 2
The zero-temperature elastic constants C_{ij} (GPa) under pressure P (GPa) for α-Ti_3GeC_2.

P	C_{11}	C_{12}	C_{13}	C_{33}	C_{44}
0	373.11	86.99	91.80	347.22	144.97
10	434.07	114.13	130.83	416.93	174.42
20	483.11	144.49	164.42	467.23	202.79
30	533.75	169.30	198.92	520.81	229.25
40	578.86	195.23	232.25	569.63	253.22
50	622.15	223.52	265.19	616.72	277.0
60	656.50	256.98	296.98	660.08	299.02
70	689.80	292.31	329.76	704.36	319.73
80	720.83	327.72	361.41	748.47	340.52
90	754.47	357.05	392.64	787.02	359.55
100	809.67	366.85	424.89	828.38	378.37

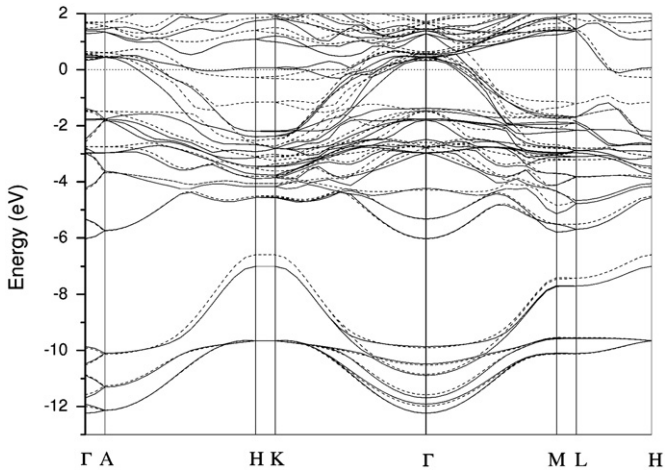

Fig. 3. The calculated electronic band structure of α- and β-Ti_3GeC_2 along some high symmetry directions of the BZ. The solid and dashed lines are for α-Ti_3GeC_2 and β-Ti_3GeC_2, respectively.

judged from the following conditions [16]:

$$\tilde{C}_{44}>0,\quad \tilde{C}_{11}>|\tilde{C}_{12}|,\quad \tilde{C}_{33}(\tilde{C}_{11}+\tilde{C}_{12})>2\tilde{C}_{13}^2 \tag{1}$$

where $\tilde{C}_{\alpha\alpha}=C_{\alpha\alpha}-P$ $(\alpha=1,2,\ldots 6)$, $\tilde{C}_{12}=C_{12}+P$, $\tilde{C}_{13}=C_{13}+P$, $\tilde{C}_{23}=C_{23}+P$. As we can see, the elastic constants in Table 2 fulfill satisfy the elastic stability criteria, which means that α-Ti_3GeC_2 is mechanically stable in the pressure range from 0 to 100 GPa. It is meaningful to discuss the B/C_{44} for this value correlates to the ductility of solids, i.e., ductile crystals are characterized by large B/C_{44} values, while brittle solids are characterized by low B/C_{44} values [17]. The B/C_{44} value of Ti_3GeC_2 is 1.3, while the value for Ti_3SiC_2, typical members of MAX compounds, is 1.7 [18], which indicates that Ti_3GeC_2 may be more brittle than Ti_3SiC_2.

3.3. Electronic properties

Fig. 3 indicates the calculated band structure along some high symmetry directions in the BZ of α-and β-Ti_3GeC_2 and the dotted lines represents the Fermi level (E_F). It can be seen that valence and conduction bands overlap considerably at the E_F and as a result there is no energy gap at E_F, which indicates that the polymorphs of Ti_3GeC_2 exhibit the metallic conductivity like other MAX compounds. Moreover, as can be seen from Fig. 3, the bands have much smaller dispersions along the *c*-axis even taking the effect of the axis-lengths into account. Furthermore, there are no valence bands crossing the E_F along the axis parallel to *c*-axis. These results indicate a strong anisotropy of the electronic properties. Such anisotropy has significant impacts on the electrical transport properties.

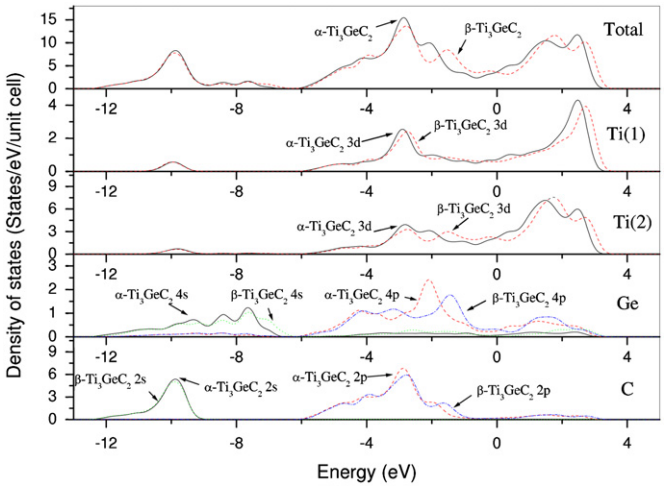

Fig. 4. The total and partial density of states for α- and β-Ti_3GeC_2.

Fig. 4 illustrates the total density of states (TDOS) and partial density of states (PDOS) of α-Ti_3GeC_2, together with that of β-Ti_3GeC_2. The valence bands of Ti_3GeC_2 can be divided into two groups, i.e., a low-energy group is dominated mainly by C 2*s* and Ge 4*s* states, and the states just below the E_F are dominated by strong covalent bonding states of the Ti 3*d* orbital and C and Si *p*-derived orbitals. The states near and above the E_F contain metallic nonbonding and antibonding Ti 3*d* orbitals. The states between −6.0 and 3.6 eV shift toward the higher energy region for β-Ti_3GeC_2, which indicates that the electronic states related to bonding are distributed in β-Ti_3GeC_2. This leads to less phase stability compared to that of α-Ti_3GeC_2.

As shown in Fig. 4, Ti_3GeC_2 exhibits metallic character with a nonzero DOS at the E_F $N(E_F)$, and the $N(E_F)$ of β-Ti_3GeC_2 has nearly the same value with that of α-Ti_3GeC_2. This indicates that the electrical conductivity of β-Ti_3GeC_2 nearly equals to that of α-Ti_3GeC_2. It can be seen from Fig. 4 that typical features of the PDOS for Ti(1) and C atoms do not change much, except for the electronic states shifting slightly toward higher energy. On the other hand, the characteristic features of the PDOS changes considerably for Ti(2) and Ge atoms. Since the electronic states obviously differ in these two polymorphs, they would expect to exhibit different mechanical properties.

4. Conclusions

In summary, we have studied the structural stability under hydrostatic pressure, electronic and elastic properties of Ti_3GeC_2 by first-principles calculations. The electronic structure of Ti_3GeC_2 shows a metallic-like character like other MAX compounds. Ti_3GeC_2 has a highly stable lattice under pressure to 100 GPa from the energy and enthalpy calculations, which is confirmed by the analysis of the variations of elastic constants with pressure, and the origin of higher structural stability was interpreted in terms of electronic level.

Acknowledgments

This work was financially supported by the Science Foundation for Youth of Liaocheng University (No. X09045). We also wish to thank referees for useful suggestions and comments.

References

[1] B. Manoun, S.K. Saxena, H.P. Liermann, R.P. Gulve, Appl. Phys. Lett. 85 (2004) 1514.
[2] R.S. Kumar, S. Rekhi, A.L. Cornelius, M.W. Barsoum, Appl. Phys. Lett. 86 (2005) 111904.
[3] B. Manoun, S.K. Saxena, M.W. Barsoum, Appl. Phys. Lett. 86 (2005) 101906.
[4] B. Manoun, S.K. Saxena, T. El-Raghy, M.W. Barsoum, Appl. Phys. Lett. 88 (2006) 201902.
[5] L. Farber, I. Levin, M.W. Barsoum, T. El-Raghy, T. Tzenov, J. Appl. Phys. 86 (1999) 2540.
[6] R. Yu, Q. Zhan, L.L. He, Y.C. Zhou, H.Q. Ye, J. Mater. Res. 17 (2002) 948.
[7] A. Onodera, H. Hirano, T. Yuasa, N.F. Gao, Y. Miyamoto, Appl. Phys. Lett. 74 (1999) 3782.
[8] J.Y. Wang, Y.C. Zhou, Phys. Rev. B 69 (2004) 144108.
[9] Z.W. Wang, C.S. Zha, M.W. Barsoum, Appl. Phys. Lett. 85 (2004) 3453.
[10] M.C. Payne, M.P. Teter, D.C. Allan, T.A. Arias, J.D. Joannopolos, Rev. Mod. Phys. 64 (1992) 1045.
[11] J.P. Perdew, K. Burke, M. Ernzerhof, Phys. Rev. Lett. 77 (1996) 3865.
[12] D. Vanderbilt, Phys. Rev. B 41 (1990) 7892.
[13] H.J. Monkhorst, J.D. Pack, Phys. Rev. B 13 (1976) 5188.
[14] F.D. Murnaghan, Finite Deformation of an Elastic Solid, John Wiley, New York, 1951.
[15] F. Birch, J. Geophys. Res. 83 (1978) 1257.
[16] G.V. Sin'ko, N.A. Smirnov, J. Phys.: Condens. Matter. 14 (2002) 6989.
[17] Z.M. Sun, D. Music, R. Ahuja, J.M. Schneider, Phys. Rev. B 71 (2005) 193402.
[18] B. Holm, R. Ahuja, B. Johansson, Appl. Phys. Lett. 79 (2001) 1450.